Journal of Computational Physics 228 (2009) 8380–8393

Contents lists available at ScienceDirect

Journal of Computational Physics

journal homepage: www.elsevier.com/locate/jcp

An Hamiltonian interface SPH formulation for multi-fluid and free surface flows

N. Grenier [a], M. Antuono [b], A. Colagrossi [b,c,*], D. Le Touzé [a], B. Alessandrini [a]

[a] Fluid Mechanics Laboratory, École Centrale Nantes, Nantes, France
[b] INSEAN, The Italian Ship Model Basin, 00128 Roma, Italy
[c] Centre of Excellence for Ship and Ocean Structures, NTNU, Trondheim, Norway

ARTICLE INFO

Article history:
Received 2 March 2009
Received in revised form 13 August 2009
Accepted 15 August 2009
Available online 21 August 2009

Keywords:
SPH
Hamiltonian particle system
Multi-fluid
Interfacial flows
Free surface flows
Non-diffusive interface

ABSTRACT

In the present work a new SPH model for simulating interface and free surface flows is presented. This formulation is an extension of the one discussed in Colagrossi and Landrini (2003) and is related to the one proposed by Hu and Adams (2006) to study multi-fluid flows. The new SPH scheme allows an accurate treatment of the discontinuity of quantities at the interface (such as the density), and permits to model flows where both interfaces and a free surface are present. The governing equations are derived following a Lagrangian variational principle leading to an Hamiltonian system of particles. The proposed formulation is validated on test cases for which reference solutions are available in the literature.

1. Introduction

Multi-fluid flows play a significant role in numerous engineering applications characterized by strong dynamics of the flow (e.g. flows involved in mixing/separation devices, engines, propellers with cavitation, etc.). With respect to this, the SPH scheme has proved to be a valuable candidate as simulation method (see for example [2,3]). Even for that flows (i.e. jets, sprays, impacts, free surface reconnections, etc.) which are generally modeled by using one-fluid SPH scheme (see e.g. [4]), the air phase can have a large influence on the flow evolution and on the subsequent loads on structures. In this context, the main advantage of the SPH model is that fluid elementary volumes are followed in their Lagrangian motion and, consequently, the interface between two fluids will remain sharply described. Hence, the interface will not be diffused like in standard mesh-based methods (Volume Of Fluids, Level-Set, Constrained Interpolation Profile, etc.).

Nonetheless, although the classical SPH formulation succeeds in correctly simulating one-fluid flows, the presence of an interface and the physical conditions associated make a stable two fluid formulation more difficult to derive. The main issue is the estimation of the ratio between the pressure gradient and the density inside the momentum equation, since the density is discontinuous when crossing the interface. Since the SPH scheme relies on a smoothing procedure (namely, each particle is associated to a compact support on which the smoothing is made), the accuracy in modeling sharp discontinuities worsens when the compact support intersects the interface. Indeed, in this eventuality, the density of the fluid on the other side of the interface spuriously influences both the local density and pressure fields and, consequently, the acceleration of the concerned particle.

* Corresponding author. Address: INSEAN, The Italian Ship Model Basin, 00128 Roma, Italy. Tel.: +39 0650299343; fax: +39 065070619.
E-mail address: a.colagrossi@insean.it (A. Colagrossi).

0021-9991/$ - see front matter © 2009 Elsevier Inc. All rights reserved.
doi:10.1016/j.jcp.2009.08.009

In the present work a new SPH formulation for simulating interface flows is presented. It is an extension of the formulation discussed in Colagrossi and Landrini [1] and it is based on the Lagrangian variational approach introduced by Bonet and Lok [5]. Following this procedure, the derived system of particles results to be Hamiltonian.

The resulting formulation presents similarities with the one proposed by Hu and Adams [2] for incompressible multi-fluid flows. However, among other differences, the present formulation permits to model multi-fluid flows together with the presence of a free surface (i.e. an interface between liquids and air where the air phase is considered as being at constant pressure with zero velocity).

Further, in the present formulation a specific attention is paid to enhance the accuracy of the scheme, especially through the use of a Shepard kernel. The latter kernel allows us to accurately preserve the discontinuity of the density across interfaces. To do so, an original variant of gradient renormalization formula of the Shepard kernel is derived, which differs from the one usually associated to this kernel in the literature [6].

After a detailed description of the proposed formulation, a number of validations are performed on test cases for which reference solutions are available in the literature. First, an air bubble rising by gravity in a water column at rest is studied providing a comparison to Level-Set simulations. Then, Rayleigh–Taylor instabilities are investigated in terms of accuracy and convergence and again compared to Level-Set simulations. Finally, the capabilities of the proposed formulation are illustrated by modeling the gravity currents generated after a lock-release. The latter case involves two different kinds of liquids and the free surface dynamics.

2. Physical model

In the present work we model the Navier–Stokes equations in the fluid domain Ω including several viscous Newtonian fluids. Fig. 1 shows that Ω is composed by different fluids $\mathcal{A}, \mathcal{B}, \ldots$ so that $\Omega = \mathcal{A} \cup \mathcal{B} \cup \ldots$. The boundaries of the domain Ω are the free surface $\partial\Omega_F$ and the solid boundaries $\partial\Omega_B$.

The conservation of the momentum in Ω is written in Lagrangian formalism as

$$\rho \frac{\mathrm{D}\mathbf{u}}{\mathrm{D}t} = -\nabla p + \mathbf{F}_\mathrm{V} + \mathbf{F}_\mathrm{S} + \mathbf{F}_\mathrm{B} \tag{1}$$

where $\mathbf{u}$, p and ρ are respectively the velocity, the pressure and the density fields, while $\mathbf{F}_\mathrm{V}, \mathbf{F}_\mathrm{S}, \mathbf{F}_\mathrm{B}$ represent the viscous, the surface tension and the external body forces.

The location of a generic material point $\mathbf{X}$ at time t is described by $\mathbf{x}(t)$ through

$$\mathbf{x}(t) = \phi(\mathbf{X}, t) \tag{2}$$

where ϕ is the map which links the Lagrangian coordinates $\mathbf{X}$ with the physical ones $\mathbf{x}$.

Weakly compressible fluids are considered. Under this assumption the pressure field can be directly linked to the density field neglecting the dependency on the specific entropy s. Therefore the fluids considered are barotropic and the equation of state reduces to $p = f(\rho)$. Here the Tait equation is considered

$$p = \frac{c_0^2 \rho_0}{\gamma}\left[\left(\frac{\rho}{\rho_0}\right)^\gamma - 1\right] \tag{3}$$

where c_0 is the speed of sound in the condition $\rho = \rho_0$. From Eq. (3) derives that the speed of sound follows a polytropic law with a characteristic exponent γ.

To verify the weakly-compressibility hypothesis, the speed of sound c_0 must be at least ten times greater than the maximum fluid velocity. Then the inequality

$$c_0 > 10 \max(|\mathbf{u}|)_\Omega \tag{4}$$

has to be always satisfied. Condition (4) guarantees that the density variations are always smaller than $1\%\rho_0$. Nonetheless, for computational and numerical reasons one generally does not use the real speed of sound of the considered fluids. This only affects the acoustics of the solution, leaving unaffected the flow evolution (see e.g. [7]). The condition (4) on the Mach number $M = |\mathbf{u}|/c < 0.1$ is thus satisfied by choosing a fictitious speed of sound.

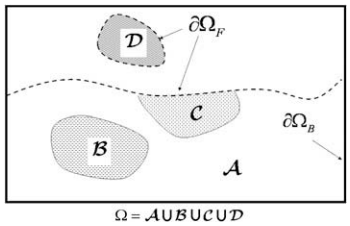

Fig. 1. Fluid domain Ω composed by different fluids $\mathcal{A}, \mathcal{B}, \ldots$

The continuity equation is written as

$$\frac{\mathrm{D}\log\mathcal{J}}{\mathrm{D}t} = \mathrm{div}(\mathbf{u}); \quad \mathcal{J} = \frac{\rho_0(\mathbf{X})}{\rho(\mathbf{X},t)} = \frac{v(\mathbf{X},t)}{v_0(\mathbf{X})} \tag{5}$$

where the Jacobian determinant $\mathcal{J}$ is linked to the map ϕ (see Eq. 2) through

$$\mathcal{J} = det(\mathbf{F}); \quad \mathbf{F} = \frac{\partial \mathbf{x}}{\partial \mathbf{X}}$$

$\mathcal{J}$ represents the ratio between the initial and the current densities, or between the specific volume and the initial one.

Summarizing, the governing equations used in this work are

$$\begin{cases} \frac{\mathrm{D}\log\mathcal{J}}{\mathrm{D}t} = \mathrm{div}(\mathbf{u}); \quad v(\mathbf{X},t) = \mathcal{J}(\mathbf{X},t)v_0(\mathbf{X}); \quad \rho(\mathbf{X},t) = \frac{1}{v(\mathbf{X},t)} \\ p(\mathbf{X},t) = \frac{c_{0\mathcal{X}}^2\rho_{0\mathcal{X}}}{\gamma_{\mathcal{X}}}\left[\left(\frac{\rho(\mathbf{X},t)}{\rho_{0\mathcal{X}}}\right)^{\gamma_{\mathcal{X}}} - 1\right]; \quad \forall \mathbf{X} \in \mathcal{X} \\ \rho\frac{\mathrm{D}\mathbf{u}}{\mathrm{D}t} = -\nabla p + \mathbf{F}_{\mathrm{V}} + \mathbf{F}_{\mathrm{S}} + \mathbf{F}_{\mathrm{B}}; \quad \frac{\mathrm{D}\mathbf{x}}{\mathrm{D}t} = \mathbf{u} \end{cases} \tag{6}$$

where $\mathcal{X}$ indicates a generic weekly-compressible fluid in the domain Ω.

Boundary conditions. Appropriate boundary conditions on $\partial\Omega = \partial\Omega_F \cup \partial\Omega_B$ have to be enforced to solve the system of partial differential Eq. (6). The fluid boundary $\partial\Omega$ is composed by a free surface $\partial\Omega_F$ and solid boundaries $\partial\Omega_B$. Along the free surface, two conditions must be verified. The kinematic condition implies that the fluid particles initially on $\partial\Omega_F$ will remain on it. If no surface tension and viscous effects are taken into account, the dynamic condition states that the pressure is continuous across $\partial\Omega_F$, therefore equal to the external pressure p_e present on the other side. When p_e is constant, a trivial change of pressure reference leads to $p = 0$ on the free surface, which is commonly used by SPH practitioners. These two conditions are implicitly verified in the SPH formalism (see [8] for an extensive discussion).

On solid boundaries $\partial\Omega_B$, a free-slip or a no-slip condition has to be modeled. A way to enforce this condition is to use a local mirroring of the flow on the other side of the solid boundary, at each time step (see [1]). Adequate (symmetric or antisymmetric) physical quantities are then given to the mirrored particles. The efficiency of this 'ghost' approach has been underlined by Monaghan in his review of the SPH method [9]. The use of this technique has been extensively validated both in terms of flow kinematics and dynamics through various applications (see e.g. [7,10,11]).

3. Principle of virtual works (PVW)

In the present section we discuss the conservation properties of the considered fluids. This can be done following a Lagrangian variational principle as done by several authors (see e.g. [9,12]), or equivalently following the variational principle used by Bonet and Lok [5]. Here we write the principle of virtual work (PVW) in its general form

$$\int_\Omega \nabla p \cdot \delta\boldsymbol{w} dV = \int_\Omega \delta\pi dm = \delta\Pi \tag{7}$$

where $\delta\pi$ is the variation of the specific internal energy due to the virtual displacement field $\delta\boldsymbol{w}$, while dm is the elementary mass ρdV. This theorem states that in absence of mechanical work due to external forces and viscous dissipations, the work done by the pressure forces due to a generic virtual displacement field $\delta\boldsymbol{w}$ has to be balanced by the total variation of the internal energy $\delta\Pi$ of the fluid-dynamic system. It must be noted that in Eq. (7) the work of the stress tensor on the free surface does not appear since it is null by definition (see [8] for a detailed discussion).

Assuming the fluid to be isentropic, the variation $\delta\pi$ is directly linked to the variation $\delta\rho$ of the density field due to the virtual displacement $\delta\boldsymbol{w}$ (see e.g. [9]):

$$\delta\pi = \frac{p}{\rho^2}\delta\rho; \quad \delta\rho = -\rho\mathrm{div}(\delta\boldsymbol{w}) \tag{8}$$

The second equation is the continuity equation expressed in terms of $\delta\rho$ and $\delta\boldsymbol{w}$.

Therefore Eq. (7) can be rewritten in the following two forms

$$\begin{aligned} &(a) \quad \int_\Omega \nabla p \cdot \delta\boldsymbol{w} dV = \int_\Omega \frac{p}{\rho^2}\delta\rho dm = \delta\Pi \\ &(b) \quad \int_\Omega \nabla p \cdot \delta\boldsymbol{w} dV = -\int_\Omega p\mathrm{div}(\delta\boldsymbol{w}) dV = \delta\Pi \end{aligned} \tag{9}$$

In [5,13] it is shown that these equalities play an important role when the governing equations are discretized on a system of particles (i.e. when the material point $\mathbf{X}$ becomes an elementary fluid volume). Indeed once the discrete form for the variation $\delta\rho$ or for the divergence operator are chosen, the discrete form for the pressure gradient ∇p has to satisfy (9), see [8]. Such a procedure ensures the system of particles to be Hamiltonian. In the next section it will be shown how this procedure can be used for deriving different SPH formulations.

4. Numerical model

4.1. Integral interpolation

In the SPH method, the fluid domain Ω is discretized in a finite number N of *particles* representing elementary fluid volumes ΔV, each one with its own local mass Δm and other physical properties. In this context a generic field f is approximated at a generic position $\mathbf{x}$ through the convolution sum

$$\langle f\rangle(\mathbf{x}) = \sum_j f_j W(\mathbf{x}-\mathbf{x}_j)\Delta V_j \tag{10}$$

where f_j is the value of f associated to the generic particle j, ΔV_j is its volume and finally $W(\mathbf{x}-\mathbf{x}_j)$ is a kernel function. In practical SPH computations, the choice of the kernel function affects both the CPU requirements and the stability properties of the algorithm. In this work a Gaussian kernel with a compact support has been adopted:

$$W_j(\mathbf{x}_i) = W(r) = \begin{cases} \frac{1}{\pi h^2}\left[\frac{e^{-(r/h)^2}-C_0}{1-C_1}\right] & \text{if } r \leqslant \delta h \\ 0 & \text{otherwise} \end{cases} \tag{11}$$

$$C_0 = e^{-\delta^2}; \quad C_1 = C_0(1+\delta^2)$$

where $r = \|\mathbf{x}_j - \mathbf{x}_i\|$ is the Euclidean distance between the two particles. The length δh represents a cut-off radius, typically set equal to $3h$ as for the classical fifth-order B-spline support [14], h is called *smoothing length* and when it goes to zero the kernel function W becomes a delta Dirac function. Note that the integration of the function (11) on its support is equal to one. Choosing $\delta = 3$ the constant C_0 and C_1 are respectively $C_0 \simeq 10^{-4}$ and $C_1 \simeq 10^{-3}$. This choice is motivated by the fact that, from a numerical point of view, the behaviour of the kernel (11) is almost identical to the classical Gaussian kernel with unbounded domain (i.e. $\delta \to \infty$). In fact, the maximum of the relative error between the two kernels is about 0.1%.

For what concerns the latter one the following properties are well established: (i) among ten tested kernel shapes, the Gaussian kernel appears to give the best numerical accuracy in the stable field [15]; (ii) the comparison of the Gaussian kernel to classically used spline kernels showed that the former leads to better stability properties [16]; (iii) it presents also a lower computational cost with respect to evolved forms of spline kernels [7]; finally (iv), its gradient can be straightforwardly obtained from the evaluation of W itself.

The spatial derivatives of the field f evaluated at the particle positions can be estimated using the formula (10)

$$\langle \nabla f\rangle(\mathbf{x}) = \sum_j (\nabla f)_j W_j(\mathbf{x})\Delta V_j \tag{12}$$

After some manipulation (for more details see [8]) it is possible to move the gradient operator to the kernel and the previous formula can be approximated by

$$\langle \nabla f\rangle(\mathbf{x}) = \sum_j f_j \nabla W_j(\mathbf{x})\Delta V_j - f(\mathbf{x})\sum_j \nabla W_j(\mathbf{x})\Delta V_j \tag{13}$$

where ∇ denotes the derivative with respect to $\mathbf{x}$. Far from the free surface the second term of Eq. (13) is small in comparison to the first one while it increases when getting closer to it; therefore this term acts as a boundary term (see [8] for more details).

One can note that this formula permits to recover exactly the null gradient of a constant function.[1]

Kernel Renormalization. The interpolation formula (10) cannot be applied to regions close to the free surface since $\Gamma(\mathbf{x}) = \sum_j W_j(\mathbf{x})\Delta V_j$ decreases there due to the absence of points on the other side of this boundary. For example, near a flat free surface $\Gamma(\mathbf{x})$ approximately gives 0.5 instead of 1. To recover an accurate interpolation a renormalization of the kernel function is introduced

$$\begin{cases} \prec f \succ (\mathbf{x}) = \sum_j f_j W_j^S(\mathbf{x})\Delta V_j; \\ W_j^S(\mathbf{x}) = \frac{W_j(\mathbf{x})}{\Gamma(\mathbf{x})}; \quad \Gamma(\mathbf{x}) = \sum_k W_k(\mathbf{x})\Delta V_k \end{cases} \tag{14}$$

where the new kernel W^S is known in the literature as *Shepard* kernel (see e.g. [6]).

Then, substituting the Shepard kernel in Eq. (12), after some manipulations we get

$$\prec \nabla f \succ (\mathbf{x}) = \frac{1}{\Gamma(\mathbf{x})}\sum_j f_j \nabla W_j(\mathbf{x})\Delta V_j - \frac{f(\mathbf{x})}{\Gamma(\mathbf{x})}\sum_j \nabla W_j(\mathbf{x})\Delta V_j \tag{15}$$

[1] Conversely, if f is linear the formula (13) does not permit to recover the exact value of the gradient, so it is complete only at zero-th order (see e.g. [6]).

It must be underlined that this form does not correspond to the one obtained after differentiation of the Shepard kernel [6]. Indeed, in the latter case one obtains

$$\sum_j f_j \nabla W_j^S(\mathbf{x}) \Delta V_j = \frac{1}{\Gamma(\mathbf{x})} \sum_j f_j \nabla W_j(\mathbf{x}) \Delta V_j - \frac{\prec f \succ (\mathbf{x})}{\Gamma(\mathbf{x})} \sum_j \nabla W_j(\mathbf{x}) \Delta V_j \tag{16}$$

which clearly differs from Eq. (15) since a Shepard interpolation of the field f appears in the second term.

Summarizing, the interpolation formulæ which will be considered in the following are

$$\begin{aligned} A &\begin{cases} \langle f \rangle(\mathbf{x}) = \sum_j f_j W_j(\mathbf{x}) \Delta V_j \\ \langle \nabla f \rangle(\mathbf{x}) = \sum_j [f_j - f(\mathbf{x})] \nabla W_j(\mathbf{x}) \Delta V_j \end{cases} \\ B &\begin{cases} \prec f \succ (\mathbf{x}) = \sum_j f_j \frac{W_j(\mathbf{x})}{\Gamma(\mathbf{x})} \Delta V_j \\ \prec \nabla f \succ (\mathbf{x}) = \sum_j [f_j - f(\mathbf{x})] \frac{\nabla W_j(\mathbf{x})}{\Gamma(\mathbf{x})} \Delta V_j \end{cases} \end{aligned} \tag{17}$$

where formulæ A are the ones usually used in the literature while formulæ B are the ones adopted in the present SPH formulation.

4.2. SPH formulations for interface flows with n-terms.

Consider a density field approximated through Eq. (10)

$$\langle \rho \rangle(\mathbf{x}) = \sum_j \rho_j W_j(\mathbf{x}) \Delta V_j \tag{18}$$

If a direct relationship between the particle mass Δm_j, density ρ_j and elementary volume ΔV_j is assumed (i.e. $\rho_j = \Delta m_j / \Delta V_j$), the formula (18) becomes

$$\langle \rho \rangle(\mathbf{x}) = \sum_j \Delta m_j W_j(\mathbf{x}) \tag{19}$$

This formula was used in the original SPH scheme and allows to evaluate the density field once the spatial distribution of the particle masses Δm_j is known. One can note that using this formula time integration of the continuity equation is not necessary. Unfortunately expression (19) is not able to represent the sharp density discontinuity across the interface between two immiscible fluids. To overcome this difficulty, a different approach is used by Hu and Adams [2] who evaluate the density field through

$$\langle \rho \rangle(\mathbf{x}_i) = \Delta m_i \sum_j W_j(\mathbf{x}_i) \tag{20}$$

or introducing a *n-term*

$$\langle \rho \rangle(\mathbf{x}_i) = \Delta m_i n_i; \quad n_i = \sum_j W_j(\mathbf{x}_i) \tag{21}$$

This formula is able to reproduce density discontinuities inside the domain Ω. Actually, the density of the generic ith particle is not influenced by the masses of its neighbors Δm_j, even though the particle i receives the geometric contribution $W_j(\mathbf{x}_i)$ from the particle j. Therefore the particles i and j can belong to different fluids without having their density unphysically affected by the other fluid close to the interface. Note that the terms n_i are purely geometrical since they are only associated to the particle spatial distribution through the kernel W.

Substituting (21) in (9), a $\delta\Pi$ becomes

$$\begin{aligned} \delta\rho_i &= \Delta m_i \sum_j \nabla W_j(\mathbf{x}_i) \cdot (\delta\mathbf{w}_i - \delta\mathbf{w}_j) \\ &\Downarrow \\ \delta\Pi &= \sum_i \tfrac{p_i}{\rho_i^2} \delta\rho_i \Delta m_i = \sum_i \tfrac{p_i}{n_i^2} \sum_j \nabla W_j(\mathbf{x}_i) \cdot (\delta\mathbf{w}_i - \delta\mathbf{w}_j) \\ &= \sum_i \langle \nabla p \rangle(\mathbf{x}_i) \cdot \delta\mathbf{w}_i \Delta V_i \end{aligned} \tag{22}$$

Similarly to the work done by Bonet and Lok [5] one can rearrange the indexes in the double summation and get the expression for the pressure gradient

$$\langle \nabla p \rangle(\mathbf{x}_i) = n_i \sum_j \left(\frac{p_i}{n_i^2} + \frac{p_j}{n_j^2} \right) \nabla W_j(\mathbf{x}_i) \tag{23}$$

Note that using such a variational principle we demonstrate that the formulation by Hu and Adams [2] leads to an Hamiltonian system of particles.

However, the density representation given in (21) cannot be used if free surfaces are present in the fluid domain Ω. In this case the density will unphysically decrease as already commented. Moreover, if particles have different sizes formula (21) cannot take into account the mass distribution. In fact, the particle i has no information about the masses of its neighbor particles and gives the same geometric weight to each of them.

4.3. Present formulation

Following [17], the proposed formulation is based on the use of a Shepard kernel for the density evaluation through

$$\begin{cases} \prec \rho \succ (\mathbf{x}) = \sum\limits_{j\in\mathcal{X}} \Delta m_j W_j^S(\mathbf{x}); \quad W_j^S(\mathbf{x}) = \frac{W_j(\mathbf{x})}{\Gamma^{\mathcal{X}}(\mathbf{x})}; \\ \Gamma^{\mathcal{X}}(\mathbf{x}) = \sum\limits_{k\in\mathcal{X}} W_k(\mathbf{x})\Delta V_k; \qquad \forall \mathbf{x} \in \mathcal{X} \end{cases} \tag{24}$$

The Shepard kernel W^S is normalized by definition and therefore the identity

$$\sum_{j\in\mathcal{X}} W_j^S(\mathbf{x})\Delta V_j = 1 \quad \forall \mathbf{x} \in \mathcal{X} \tag{25}$$

is always satisfied and does not depend on the number of particles. The summation for calculating the term $\Gamma^{\mathcal{X}}(\mathbf{x})$ is extended only to the particles belonging to the fluid $\mathcal{X}$ containing the point $\mathbf{x}$. For this reason, in (24) and (25) the indices in the summation are restricted to the particles belonging to the generic fluid $\mathcal{X}$. In this way the discontinuities of the density field are treated explicitly.

Note that the density representation (24) is conceptually different from formula (19) since the Shepard kernel W^S is function of the particle volume distribution ΔV. Thus, one needs to know the volume distribution to perform the density evaluation through Eq. (24). A way to obtain this volume distribution could be to use a tessellation. However, this procedure would be complex and costly, so here we prefer to obtain the volumes through their time evolution given by the continuity Eq. (5).

As a consequence, the use of Eq. (24) leads to a *relaxed link* between the mass Δm_i, volume ΔV_i and density ρ_i of the generic ith particle. Therefore, the direct link $\Delta m_i = \rho_i \Delta V_i$ is not used anymore.

Then, to be consistent with the fact that the density is evaluated thanks to a Shepard renormalization we evaluate the divergence of the velocity as

$$\prec \mathrm{div}(\mathbf{u}) \succ_i = \frac{1}{\Gamma_i} \sum_j (\mathbf{u}_j - \mathbf{u}_i) \cdot \nabla W_j(\mathbf{x}_i) \Delta V_j \tag{26}$$

where the summation is extended to the whole particle neighbourhood. In this way the discontinuity of the tangential velocity field at the interface will be regularized by Eq. (26). Conversely, as already stressed, the density discontinuities are explicitly treated through Eq. (24).

Substituting the form (26) of the divergence operator in (9,b) $\delta\Pi$ becomes

$$\delta\Pi = -\sum_i p_i \prec \mathrm{div}(\delta\mathbf{w}) \succ_i \Delta V_i = \sum_i \frac{p_i}{\Gamma_i} \left[\sum_j (\delta\mathbf{w}_i - \delta\mathbf{w}_j) \cdot \nabla W_j(\mathbf{x}_i) \Delta V_j \right] \Delta V_i = \sum_i \prec \nabla p \succ_i \cdot \delta\mathbf{w}_i \Delta V_i \tag{27}$$

which leads to a new discrete formula for the smoothed pressure gradient $\prec \nabla p \succ$

$$\prec \nabla p \succ_i = \sum_j \left(\frac{p_i}{\Gamma_i} + \frac{p_j}{\Gamma_j} \right) \nabla W_j(\mathbf{x}_i) \Delta V_j \tag{28}$$

Summarizing, the formulation proposed in this work discretizes the continuum system of governing Eq. (6) in the following way: at the generic time t, the positions, masses and volumes of the particles are known and, therefore, it is possible to evaluate the following quantities

$$\begin{cases} \Gamma_i^{\mathcal{X}} = um_{k\in\mathcal{X}} W_k(\mathbf{x}_i) \Delta V_k \\ \prec \rho \succ_i = \frac{\sum_{j\in\mathcal{X}} \Delta m_j W_j(\mathbf{x}_i)}{\Gamma_i^{\mathcal{X}}} \\ p(\mathbf{x}_i) = \frac{c_{0\mathcal{X}}^2 \rho_{0\mathcal{X}}}{\gamma_{\mathcal{X}}} \left[\left(\frac{\prec \rho \succ_i}{\rho_{0\mathcal{X}}} \right)^{\gamma_{\mathcal{X}}} - 1 \right]; \quad \forall \mathbf{x}_i \in \mathcal{X} \end{cases} \tag{29}$$

After the updated density and pressure distributions are known, the fundamental time derivatives can be evaluated by

$$\begin{cases} \frac{D\mathbf{x}_i}{Dt} = \mathbf{u}_i \\ \frac{D\log \mathcal{J}_i}{Dt} = \sum_j (\mathbf{u}_j - \mathbf{u}_i)\cdot \frac{\nabla W_j(\mathbf{x}_i)}{\Gamma_i}\Delta V_j \\ \prec \rho \succ_i \frac{D\mathbf{u}_i}{Dt} = -\sum_j \left(\frac{p_i}{\Gamma_i}+\frac{p_j}{\Gamma_j}\right)\nabla W_j(\mathbf{x}_i)\Delta V_j + \mathbf{F}_V + \mathbf{F}_S + \mathbf{F}_B \end{cases} \tag{30}$$

Finally, using these time derivatives it is possible to update volumes, velocities and positions of the particle system. The masses Δm_i are fixed (that is, they do not change in time) and, therefore, the global mass of the system is preserved. Further, the pressure gradient formulation, being obtained through the PVW, preserves both linear and angular momenta. With respect to this, $\mathbf{F}_V$ and $\mathbf{F}_S$ have to be properly chosen since not all the formulations available in the literature are conservative. Anyway, we postpone this facet in the following section. Once again, we underline that the present scheme allows modeling both interfaces and free surfaces; note that if one considers only one fluid it simplifies as $\Gamma_i^{\mathcal{X}} = \Gamma_i$.

4.3.1. Viscous and surface tension forces

Regarding the viscous and surface tension forces, the work by Hu and Adams [2] can be adapted to the present formulation, as shown in this section. However since in the present work we are not dealing with flows in which surface tension plays a relevant role, we postpone a detailed analysis of the surface tension formulation to a future work.

Following Flekkøy et al. [18,2] the inter-particle averaged shear tensor $\mathbf{T}_{ij}^V$ whose compressible part is neglected can be approximated as

$$\mathbf{T}_{ij}^V = \frac{2\mu_i\mu_j}{\mu_i+\mu_j}\frac{1}{r_{ij}^2}[(\mathbf{x}_i-\mathbf{x}_j)\otimes(\mathbf{u}_i-\mathbf{u}_j)+(\mathbf{u}_i-\mathbf{u}_j)\otimes(\mathbf{x}_i-\mathbf{x}_j)] \tag{31}$$

where μ is the dynamic viscosity coefficient and r_{ij} is the distance between particles i and j. The viscous force $\mathbf{F}^V$ acting on the generic particle i can be evaluated through the discrete formula

$$\mathbf{F}_i^V = \frac{1}{2}\sum_j \left(\frac{1}{\Gamma_i}+\frac{1}{\Gamma_j}\right)\mathbf{T}_{ij}^V \nabla W_j(\mathbf{x}_i)\Delta V_j \tag{32}$$

Neglecting again the compressibility effects, this formula can be rewritten as (for details see [2])

$$\mathbf{F}_i^V = \sum_j \frac{2\mu_i\mu_j}{\mu_i+\mu_j}\left(\frac{1}{\Gamma_i}+\frac{1}{\Gamma_j}\right)\frac{(\mathbf{x}_i-\mathbf{x}_j)\cdot\nabla W_j(\mathbf{x}_i)}{r_{ij}^2}(\mathbf{u}_i-\mathbf{u}_j)\Delta V_j \tag{33}$$

which resembles a mixing of the formulæ adopted by Morris et al. [19] and Monaghan [9] with the presence of the corrective term $[1/\Gamma_i + 1/\Gamma_j]$. Anyway, differently from the equation proposed by Monaghan [9] (33), does not preserve the angular momentum. A possible adaptation of the Monaghan formula to the present formulation is

$$\mathbf{F}_i^V = \sum_j \frac{8\mu_i\mu_j}{\mu_i+\mu_j}\left(\frac{1}{\Gamma_i}+\frac{1}{\Gamma_j}\right)\frac{(\mathbf{x}_i-\mathbf{x}_j)\cdot(\mathbf{u}_i-\mathbf{u}_j)}{r_{ij}^2}\nabla W_j(\mathbf{x}_i)\Delta V_j \tag{34}$$

The expression (34) still preserves linear and angular momenta and, for this reason, is used in all the test cases shown in the present work. Note that without the corrective term $[1/\Gamma_i + 1/\Gamma_j]$ in formulæ (33) and (34), the viscous force unphysically decreases close to the free surface as shown in [20].

To model the surface tension, a continuous surface force (CSF) model [21] can be adopted. To simplify the notation we consider only two fluids $(\mathcal{X},\mathcal{Y})$ here. The surface tension $\mathbf{F}_{Si}^{\mathcal{X}\mathcal{Y}}$ acting on the generic ith particle belonging to the fluid $\mathcal{X}$ due to the presence of $\mathcal{Y}$, can be evaluated by

$$\begin{cases} \mathbf{F}_{Si}^{\mathcal{X}\mathcal{Y}} = \mathrm{div}(\mathbf{T}_{Si}^{\mathcal{X}\mathcal{Y}}) \quad \forall i \in \mathcal{X} \\ \mathbf{T}_{Si}^{\mathcal{X}\mathcal{Y}} = \sigma^{\mathcal{X}\mathcal{Y}}\frac{1}{|\nabla C_i|}\left(\frac{\mathbb{I}}{d}|\nabla C_i|^2 - \nabla C_i\otimes\nabla C_i\right) \end{cases} \tag{35}$$

where $\mathbf{T}_{Si}^{\mathcal{X}\mathcal{Y}}$ is the surface stress tensor and $\sigma^{\mathcal{X}\mathcal{Y}}$ is the surface tension coefficient between the fluids $\mathcal{X}$ and $\mathcal{Y}$; d is the spatial dimension of the problem. The tensor $\mathbf{T}_{Si}^{\mathcal{X}\mathcal{Y}}$ can be evaluated through the spatial gradient of a color index C which has a unit jump across the interface between $\mathcal{X}$ and $\mathcal{Y}$

$$C_i^{\mathcal{Y}} = \begin{cases} 0 & i \in \mathcal{X} \\ 1 & i \in \mathcal{Y} \end{cases} \tag{36}$$

In the present formulation this gradient $\nabla C_i^{\mathcal{X}\mathcal{Y}}$ can be evaluated as

$$\nabla C_i^{\mathcal{XY}} = \sum_{j\in Y}\left(\frac{C_i^{\mathcal{Y}}}{\Gamma_i}+\frac{C_j^{\mathcal{Y}}}{\Gamma_j}\right)\nabla W_j(\mathbf{x}_i)\Delta V_j, \quad \forall i\in\mathcal{X} \tag{37}$$

where $C_i^{\mathcal{Y}}=0$ by definition since particle i belongs to fluid $\mathcal{X}$. Note that this formulation provides surface tension effects between two different fluids but it does not produce any surface tension on a free surface (where ∇C becomes zero). Finally, the divergence of the surface stress tensor $\mathbf{T}_{Si}^{\mathcal{XY}}$ is evaluated through a discrete operator similar to the one used for the pressure gradient (see second Eq. (28))

$$\mathbf{F}_{Si}^{\mathcal{XY}} = \mathrm{div}(\mathbf{T}_{Si}^{\mathcal{XY}}) = \sum_j\left(\frac{\mathbf{T}_{Si}^{\mathcal{XY}}}{\Gamma_i}+\frac{\mathbf{T}_{Sj}^{\mathcal{XY}}}{\Gamma_j}\right)\nabla W_j(\mathbf{x}_i)\Delta V_j \tag{38}$$

For interface flows where surface tension effects are negligible a spurious fragmentation of the interface can take place. To prevent this, a small repulsive force is introduced in the pressure gradient

$$\nabla p_i = \sum_j\left(\frac{p_i}{\Gamma_i}+\frac{p_j}{\Gamma_j}\right)\nabla W_j(\mathbf{x}_i)\Delta V_j + \epsilon_I\sum_{j\in\mathcal{X}^C}\left(\left|\frac{p_i}{\Gamma_i}\right|+\left|\frac{p_j}{\Gamma_j}\right|\right)\nabla W_j(\mathbf{x}_i)\Delta V_j \quad \forall i\in\mathcal{X} \tag{39}$$

where ϵ_I ranges between 0.01 and 0.1, and the second summation applies to all the particles which do not belong to the fluid of the ith particle; the latter set of particles is noted by $\mathcal{X}^C$.

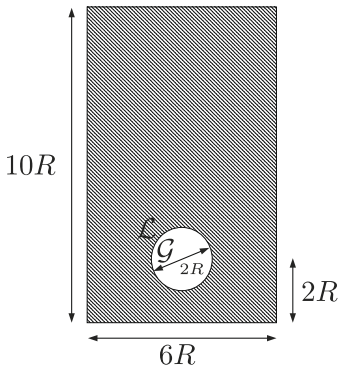

Fig. 2. Initial fluid domain.

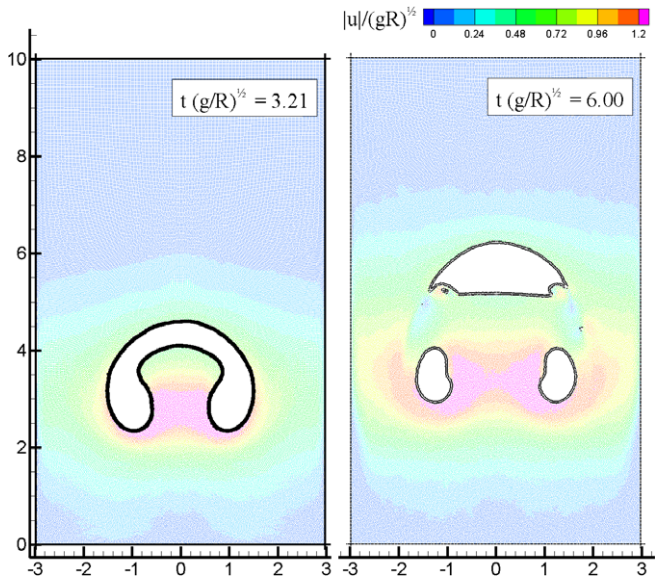

Fig. 3. Interface location and velocity field at two different times.

5. Validation results

5.1. Air bubble rising in water

We consider an air bubble rising in water at rest in a closed domain. The present formulation results are compared to those by Sussman et al. [22], obtained by solving the problem on a fixed grid with a Level-Set algorithm to capture the air–water interface.

The flow is characterized by the following dimensionless Reynolds $Re = \sqrt{(2R)^3 g}/\nu_{\mathcal{L}} = 1000$ and Bond $Bo = 4\rho_{\mathcal{L}} g R^2/\sigma = 200$ numbers, where $\mathcal{L}$ stands for liquid. Since the latter is quite large the surface tension effects can be ne-

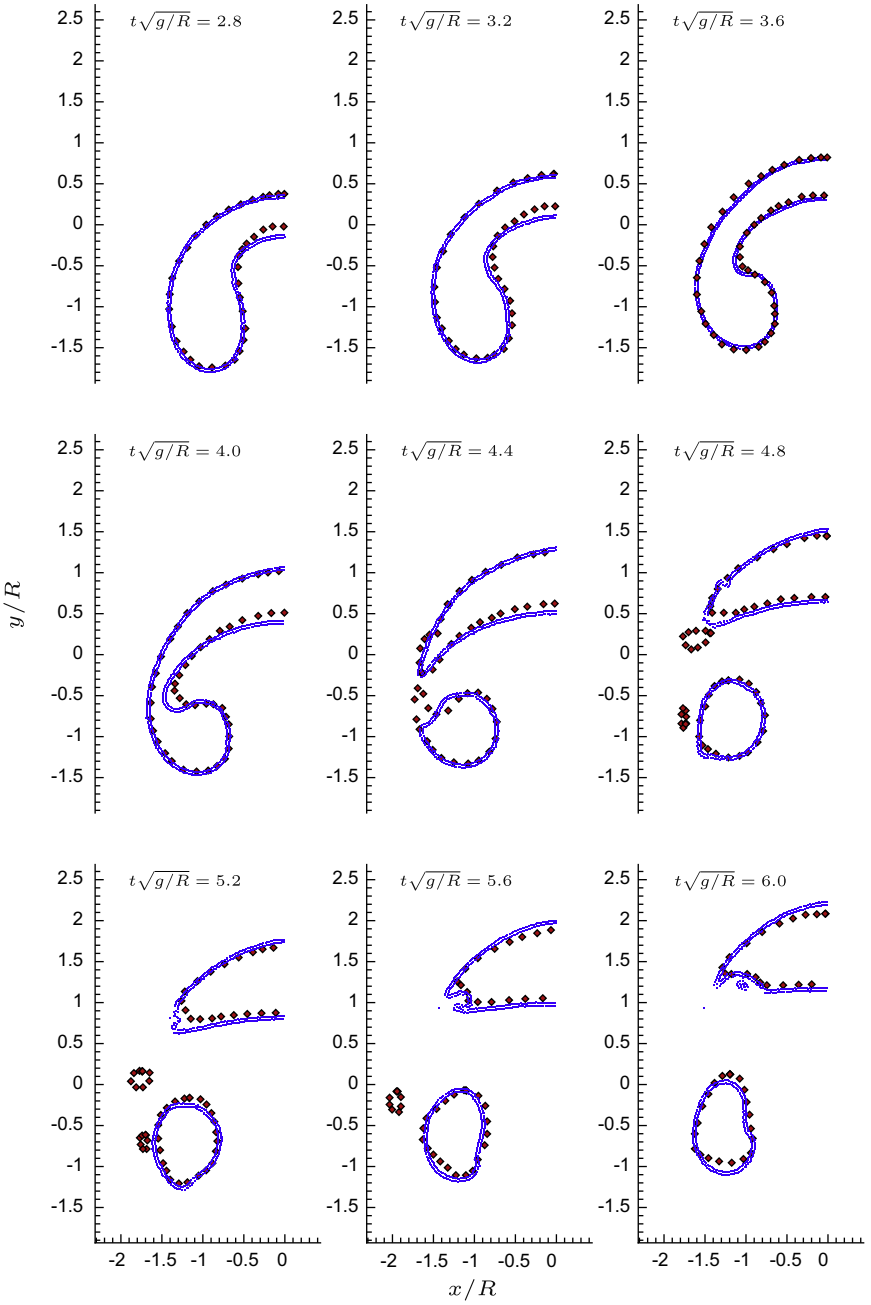

Fig. 4. Air bubble rising in water. Blue squares correspond to the present SPH model and red diamonds to the Level-Set solution in [22]. (For interpretation of the references to colour in this figure legend, the reader is referred to the web version of this article.)

glected. The two fluids are defined by their density $\rho_{\mathcal{G}}/\rho_{\mathcal{L}} = 0.001$ and kinematic viscosity $v_{\mathcal{G}}/v_{\mathcal{L}} = 128$ ratios, where $\mathcal{G}$ stands for gas. The domain is ten bubble radius high and six radius wide. The initial configuration is shown in Fig. 2. Particles are initially distributed on a regular lattice. Three spatial resolutions have been run. Results shown in Figs. 3 and 4 are for the finest one $\Delta x/R = 0.025$. The gas has a sound speed equal to $c_{\mathcal{G}} = 198\sqrt{gR}$ while the liquid one is $c_{\mathcal{L}} = 14\sqrt{gR}$. Polytropic constants are equal to $\gamma_{\mathcal{L}} = 7$ for the liquid and $\gamma_{\mathcal{G}} = 1.4$ for the gas. The parameter ϵ_I of Eq. (39) is set to 0.08 for this case.

Fig. 3 shows the bubble shape evolution and velocity magnitudes while it raises in the water column. The bubble shows a strong deformation to take a horseshoe shape, and eventually splits into three main parts. This evolution is further analyzed in Fig. 4 where the comparison between the present results and the Level-Set ones are shown at 9 different times. A good agreement is found between the two sets of results at all the instants shown. Some details are different due to the different nature of the two numerical schemes. It must be noted that the SPH results are convergent in space (an example of convergence of the model is shown on the next validation test case).

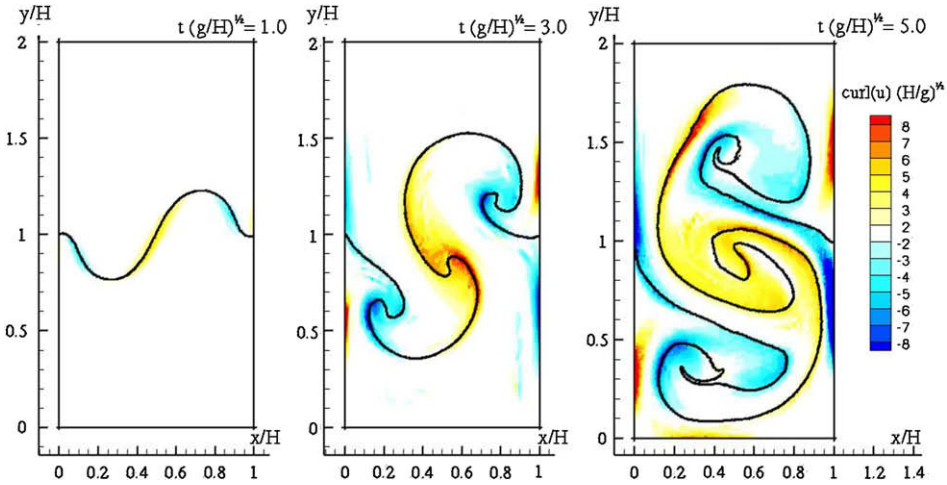

Fig. 5. Vorticity of the present SPH formulation.

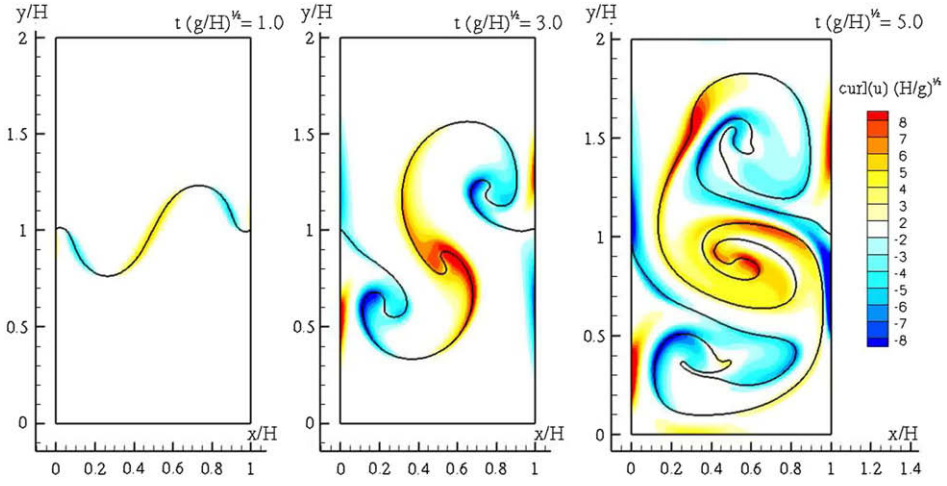

Fig. 6. Vorticity of the Level-Set formulation.

5.2. Rayleigh–Taylor instabilities

In the present section we consider the problem of the Rayleigh–Taylor instability as this test case requires an accurate modeling of the interface between two different fluids.

For SPH solutions with incompressible formulations we address the reader to the works of Cummins and Rudman [23] and Hu and Adams [3].

The computation domain is rectangular (twice as high as long) with particles initially distributed on a regular lattice. The domain is initially composed of two fluids separated by an interface located at $y = 1 - \sin(2\pi x)$. In the lower part lies a light fluid $\mathcal{X}$ of density $\rho_{\mathcal{X}} = 1$ while the heavy fluid $\mathcal{Y}$ above the interface is of density $\rho_{\mathcal{Y}} = 1.8$. The Reynolds number is $Re = \sqrt{(H/2)^3 g}/\nu = 420$ based on the half-height $H/2$ of the domain and on an equal kinematic viscosity ν for both fluids. In the state equation $\gamma = 7$ for both fluids. The coefficient ϵ_I is set equal to 0.01. Variations of this parameter (between 0.005 and 0.02) show negligible effects on the solution. No-slip conditions are enforced on the solid boundaries through ghost particles by mirroring both the normal and tangential velocities (see for example [19,24]).

Since the vorticity is generated at both the interface between the two fluids and in the boundary layer on the solid wall, the flow evolution is very complex, as shown in Fig. 5. In this figure, the present SPH formulation is compared to a reference solution given by a Level-Set solver [25] at three different times of the evolution. Both results exhibit similar vorticity patterns and interface shapes (see Figs. 5 and 6) even though local differences are visible. In particular, the SPH vorticity contour is more noisy due to the particle disorder. For what concerns the intensity of the vorticity, the two solvers predict quite similar values even if in some fluid regions the Level-Set solution shows a more intense field. This leads to a larger roll-up of the interface at the center of the domain with respect to the one obtained by the SPH scheme.

Fig. 7 shows the spatial convergence of the two models by using three different resolutions. Both methods converge and the main differences between the two solutions are concentrated in the area of higher gradients. Nonetheless the ways in which the SPH and Level-Set models converge are quite different. The SPH convergence rate is clearly faster than the Level-Set method. Actually, if one considers the coarsest resolution, the SPH solution already presents formed roll-ups close to the ones of the finest resolution.

Besides, it must be noted that the results obtained with the proposed method are much closer to reference solutions (Level-Set here or Marker-And-Cell in [23]) than previously published SPH results (see e.g. the incompressible solutions in [3] and [23]).

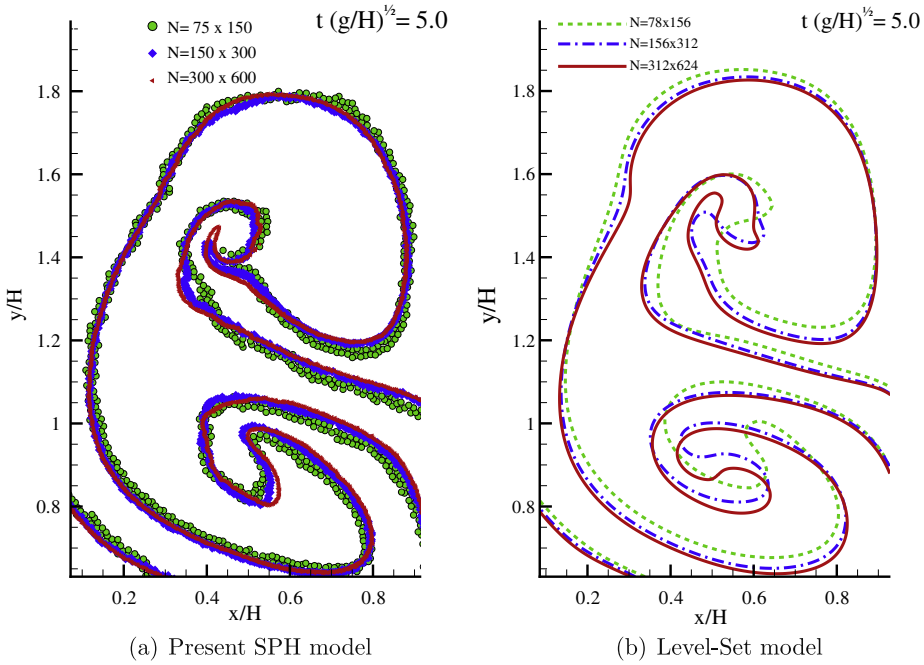

Fig. 7. Spatial convergence of Rayleigh–Taylor instabilities. Left: Present SPH model. Right: NS–LS solver.

5.3. Lock-release gravity currents

To illustrate the ability of the present model to simulate flows involving both multi-fluids and a free surface, we consider the gravity currents resulting from the instantaneous release of a dense fluid initially at rest behind a lock gate into a less dense fluid.

Two configurations are first considered with the same initial geometry but with different density and viscosity ratios. In the two cases, which are presented in Fig. 8, the heavier fluid $\mathcal{X}$ presents an evolution similar to a dam break flow. Actually, after the release of the gate, a tongue of fluids propagates at a velocity close $\sqrt{gH}$ where H is the initial fluid height. Nonetheless, due to the presence of the lighter fluid $\mathcal{Y}$, the heavier fluid front is rounded and its velocity decreases in time. Increasing the density ratio the heavier fluid front is faster, as expected, and its shape is more rounded. This is due to more intense shear effects as it is visible through the velocity contours drawn in Fig. 10. At the instants plotted in this figure, the front velocities are about 50% and 80% of $\sqrt{gH}$, respectively for the lower and higher density ratios. The gravity currents also induce a motion of the free surface which is more intense when the density ratio increases.

A third configuration is presented in Fig. 9. Here we use the same parameters of the configuration already described but set an higher column of heavier fluid behind the gate. This higher amount of fluid $\mathcal{X}$ generates more intense gravity currents as it is exhibited in Fig. 10 which shows a detail of the flow in the vicinity of the front. This induces large motions of the free surface leading to a violent sloshing flow where the two fluids are partially mixed, as illustrated in Fig. 9.

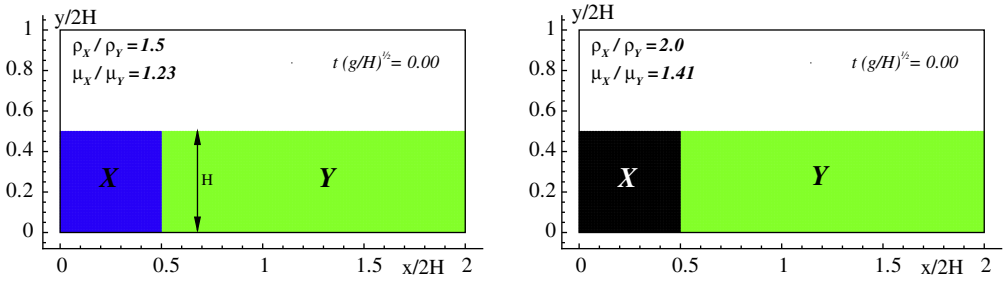

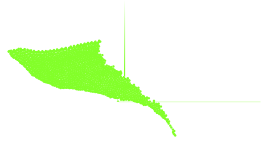

6. Conclusion

A new SPH formulation for simulating interface flows has been presented. It has been derived following a Lagrangian variational approach resulting in an Hamiltonian system of particles. When deriving this formulation a specific care has been paid to preserve an accurate description of the fields close to the interface. In particular, a renormalization procedure is used to ensure the preservation of the discontinuity of the density across the interface. This formulation is also characterized by the fact that it permits to model multi-fluid flows together with the presence of a free surface.

After a detailed description of the proposed formulation, a number of test cases have been performed on three different test cases. An air bubble rising by gravity in a water column at rest has first been studied. A good agreement has been found in comparison to the Level-Set simulation available in the literature. Then, Rayleigh–Taylor instabilities have been investigated in terms of accuracy and convergence. The comparison with a reference Level-Set solution has shown the quick convergence of the proposed formulation, and its capability to accurately describe such a complex interface evolution. The results obtained are more accurate than previously published SPH simulations [3,23]. Finally, the capabilities of the present formulation have been further illustrated on lock-release gravity currents cases. Three different configurations have been studied in terms of gravity currents intensity and resulting free surface motion. The influence of the density ratio has been investigated as well as the one of the amount of heavier fluid initially behind the gate, leading in some cases to strong sloshing with mixing of the two fluids.

Acknowledgment

The research leading to these results has received funding from the European Community's Seventh Framework Programme (FP7/2007-2013) under Grant Agreement No. 225967 "NextMuSE".

This work was also partially supported by the Centre of Excellence for Ship and Ocean Structures of NTNU Trondheim (Norway) within the "Violent Water–Vessel Interactions and Related Structural Load" project.

Author N. Grenier was granted by a CIFRE Ph.D. convention with SAIPEM S.A.

Finally, the authors would like to thank Dr. Giuseppina Colicchio for performing the Level-Set simulations shown in the present paper and for her usefull comments and suggestions.

References

[1] A. Colagrossi, M. Landrini, Numerical simulation of interfacial flows by smoothed particle hydrodynamics, J. Comput. Phys. 191 (2003) 448–475.
[2] X.Y. Hu, N.A. Adams, A multi-phase SPH method for macroscopic and mesoscopic flows, J. Comput. Phys. 213 (2006) 844–861.
[3] X.Y. Hu, N.A. Adams, An incompressible multi-phase SPH method, J. Comput. Phys. 227 (2007) 278–364.
[4] M. Landrini, A. Colagrossi, M. Greco, M.P. Tulin, Gridless simulations of splashing processes and near-shore bore propagation, J. Fluid Mech. 591 (2007) 183–213.
[5] J. Bonet, T.-S.L. Lok, Variational and momentum preservation aspects of SPH formulations, Comput. Meth. Appl. Mech. Engrg. 180 (1999) 97–115.
[6] T. Belytschko, Y. Krongauz, J. Dolbow, C. Gerlach, On the completeness of meshfree particle methods, Int. J. Numer. Meth. Engrg. 43 (1998) 785–819.
[7] A. Colagrossi, A meshless lagrangian method for free – surface and interface flows with fragmentation, Ph.D. thesis, University of Rome La Sapienza, Italy (2005) (http://padis.uniroma1.it).
[8] A. Colagrossi, D. Le Touzé, M. Antuono, Theoretical considerations on the free surface role in the SPH model, Phys. Rev. E 79/5 (2009). 056701:1-13.
[9] J.J. Monaghan, Smoothed particle hydrodynamics, Rep. Prog. Phys. 68 (2005) 1703–1759.
[10] G. Colicchio, A. Colagrossi, M. Greco, M. Landrini, Free-surface flow after a dam break: a comparative study, Ship Tech. Res. 49-3 (2002) 95–104.
[11] G. Oger, M. Doring, B. Alessandrini, P. Ferrant, Two-dimensional SPH simulations of wedge water entries, J. Comput. Phys. 213-2 (2006) 803–822.
[12] D.J. Price, Modelling discontinuities and Kelvin–Helmholtz instabilities in SPH, J. Comput. Phys. 227-24 (2008) 10040–10057.
[13] J. Bonet, M.X. Rodriguez-Paz, Hamiltonian formulation of the variable-h SPH equations, J. Comput. Phys. 209-2 (2005) 541–558.
[14] J.J. Monaghan, Smoothed particle hydrodynamics, Ann. Rev. Astron. Astrophys. 30 (1992) 543–574.
[15] J. Hongbin, D. Xin, On criterions for smoothed particle hydrodynamics kernels in stable field, J. Comput. Phys. 202 (2005) 699–709.
[16] J.P. Morris, Analysis of smoothed particle hydrodynamics with applications, PhD Thesis, Monash University, Australia, 1996.
[17] P.W. Randles, L.D. Libersky, Smoothed particle hydrodynamics: some recent improvements and applications, Comput. Meth. Appl. Mech. Engng. 139 (1996) 375–408.
[18] E.G. Flekkøy, P.V. Coveney, G. de Fabritiis, Foundations of dissipative particle dynamics, Phys. Rev. E 62-2 (2000) 2140–2157.
[19] J.P. Morris, P.J. Fox, Y. Zhu, Modeling low Reynolds number incompressible flows using SPH, J. Comput. Phys. 136-1 (1997) 214–226.
[20] A. Colagrossi, L. Delorme, J.L. Cercós-Pita, A. Souto-Iglesias, Influence of Reynolds number on shallow sloshing flows, in: Proceedings of the Third International SPHERIC Workshop, Lausanne, Switzerland, 2008.
[21] B. Lafaurie, C. Nardone, R. Scardovelli, S. Zaleski, G. Zanetti, Modelling merging and fragmentation in multiphase flows with SURFER, J. Comput. Phys. 113-1 (1994) 134–147.
[22] M. Sussman, P. Smereka, S. Osher, A level set approach for computing solutions to incompressible two-phase flow, J. Comput. Phys. 114 (1994) 146–159.
[23] S.J. Cummins, M. Rudman, An SPH projection method, J. Comput. Phys. 152 (1999) 584–607.
[24] H. Takeda, S.M. Miyama, M. Sekiya, Numerical simulation of viscous flow by smoothed particle hydrodynamics, Prog. Theor. Phys. 116 (1994) 123–134.
[25] G. Colicchio, Violent disturbance and fragmentation of free surfaces, Ph.D. Thesis, University of Southampton, UK, 2004.